JOURNAL OF CATALYSIS 105, 39–54 (1987)

Kinetic Studies on the Mechanism of the Catalytic Ethene Oxidation

R. HAUL AND G. NEUBAUER

Institut für Physikalische Chemie und Elektrochemie, Universität Hannover, D-3000 Hannover 1, Federal Republic of Germany

Received June 11, 1986; revised November 18, 1986

The kinetics of ethene oxidation catalyzed by an oxygen-preconditioned silver foil has been measured with an ultrahigh-vacuum-compatible flow reactor, using mass spectrometric gas analysis. The gradient-free reactor consisted of two concentric quartz tubes, forming a jacket of small width, covered with the catalyst. Additional temperature-programmed desorption studies and experiments with selected different types of oxygen species confirmed that only adsorbed atomic oxygen is reactive and that an oxidic surface layer is required for stable and high selectivity. Isothermal (typically 250°C, 26 mbar; 1 mbar = 100 N m^{-2}) batch and flow as well as temperature-programmed reaction measurements were evaluated by means of the Horiuti–Temkin procedure. The selectivity behavior is correctly described by the kinetic model. Rate constants and the estimated overall apparent activation energy are discussed with respect to the suggested reaction mechanism.

I. INTRODUCTION

The application of single crystal ultrahigh-vacuum (UHV) surface analysis techniques marked a turn in the long series of studies on the mechanism of the catalytic ethene oxidation. In particular, the direct coupling of a high-pressure reactor with an UHV analysis system, by means of special devices, promised a conclusive elucidation of the reaction mechanism. However, the most recent and extensive studies in this area arrived at conflicting results. The basic question in all discussions on this topic is still left unanswered. Campbell *et al.* (*1a, c*) favor a mechanism involving molecularly adsorbed oxygen and adsorbed ethene (E) in a common rate-determining step both for ethene oxide (EO) and total oxidation. On the other hand Grant and Lambert (*4, 5*) conclude that only adsorbed atomic oxygen is reactive and responsible for both EO and CO_2 production.

On the basis of kinetic and temperature-programmed desorption (TPD) studies we arrived at the same conclusions as the latter authors (*6, 7*). The results showed, however, that besides the adsorbed atomic oxygen species an oxidic layer on top of the Ag surface plays an important role for high and stable selectivity for EO production. The participation of subsurface oxygen besides adsorbed atomic oxygen has recently also been stressed again by van Santen *et al.* (*8*) on the basis of oxygen isotope experiments. In the meantime we have carried out further kinetic experiments, using an UHV-compatible flow reactor with an unpromoted polycrystalline silver foil as catalyst. The experimental data were treated by a kinetic model by means of the Horiuti–Temkin procedure.

II. EXPERIMENTAL

1. Reactor. The main features of the UHV-compatible reactor are (i) the applicability in a wide range of pressures $10^{-6} \leqq p$ (mbar) $\leqq 10^3$, (ii) continuous *in situ* mass spectrometric analysis of gas composition, (iii) negligible pressure gradient in flow experiments, (iv) small reactor volume (30 ml), (v) good contact between the gas phase and the catalyst surface, and (vi) an unpromoted Ag foil catalyst.

The reactor (*9*) consisted of two concentric quartz tubes, forming a jacket 3 mm

0021-9517/87 $3.00

wide (length 200 mm, inner diameter of outer tube 20 mm). The inner walls were covered with a silver foil, positioned by means of quartz springs (foil thickness 0.1 mm, geometric surface area 200 cm^2). The temperatures of the two externally heated silver foils were controlled within ± 1°C. An otherwise identical reference reactor without catalyst was used for calibration purposes of the mass spectrometric gas analyzer.

Batch as well as flow experiments were carried out, using calibrated UHV leak valves to adjust the flow rates of the gases or gas mixtures (C_2H_4, O_2, Ar). Glass capillary leaks of suitable width installed at the exit of the reactor and of reference reactor served to reduce the pressure at reaction conditions to the operating pressure of the mass spectrometer.

2. Mass spectrometric analysis. Gas analysis was achieved by means of an omegatron mass spectrometer with gold-plated components (*10*). This type of cyclotron resonance spectrometer is virtually free of memory effects and is particularly suitable for the mass range under consideration. Since the spectrometer is installed in a glass bulb of small volume (120 ml), kept at 250°C, detrimental adsorption effects are considerably smaller than in the case of the larger metal surfaces of conventional mass spectrometers. A scanner enabled the recording of six characteristic masses so that the concentration of all components could be continuously followed.

Extensive calibration measurements were carried out in order to convert the intensities of individual fragments into partial pressures of the particular component. Different ionization probabilities were taken into account by reference to inert Ar. For EO, fragment $m/e = 29$ contributions from ethene were allowed for, correspondingly for CO_2 a EO contribution of $m/e = 44$.

3. TPD apparatus. In order to achieve high sensitivity, the volume of the essential part of the apparatus was kept as small as possible (15 ml) and could be heated up to 500°C, basic pressure 10^{-8} mbar. The Ag foil (0.1 mm thick, 1×1 cm) was fastened to a thin quartz frame and positioned at a distance of 5 mm behind a planar window in a quartz glass tube. A quartz capillary leak, mounted at a distance of 1 mm from the Ag foil, was used to reduce the pressure for gas analysis by means of a quadrupole mass spectrometer, fitted with a scanner. The Ag foil was externally heated with a 250-W IR point glow lamp, enabling heating rates in the range $0.4 \leqq \beta/°C\ s^{-1} \leqq 17$. For temperature measurement and control, a NiCr–Ni thermocouple was fastened to the Ag foil with a thin Ag wire.

4. Substances. Ag foil was 99.999% pure (Degussa, Frankfurt). High purity (99.995%) gases were used; EO was 99.8% pure.

III. RESULTS

1. TPD Experiments

The silver foil was pretreated: H_2 (500°C), alternate evacuation, and O_2 (0.2 mbar, 350°C, 6 h); between experiments, each consisting of several dosing and TPD cycles, evacuation (10^{-8} mbar). In the TPD runs after reaching 500°C, this temperature was kept constant.

At an adsorption temperature $T_a = 150$°C (Fig. 1a) and relatively low doses, a peak (β) is shown at $T_m = 585$ K, assigned to atomic oxygen O(a) (e.g., *4, 13, 11*). After several cycles the peak height is constant, while overlap with a higher temperature peak (γ) is noticeable. In the absence of overlap the shape is symmetrical, indicating second-order desorption. Since in this case a shift of T_m to lower temperatures with increasing Θ is to be expected, the observed constancy (Fig. 1a) requires interpretation.

It turns out that the adsorption temperature has a decisive influence. At $T_a \simeq 25$°C, a shift to higher temperatures has been observed (*13, 11*). This has been explained by a net attractive interaction energy of 14 kJ/mol between O(a) (*13, 14*).

At higher dosing temperatures two peaks in the β range have been observed: (a) Ag wire, $T_a = 150$°C, O_2 6×10^{-7} mbar, 2×10^3

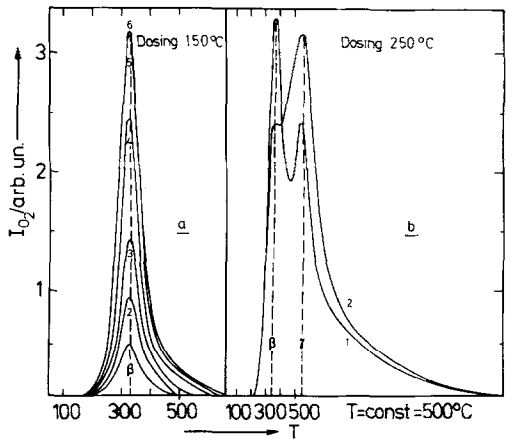

FIG. 1. TPD spectra of adsorbed atomic (β) and dissolved lattice (γ) oxygen. O_2 dosing: 0.1 mbar (a) 150°C, 1.4×10^8 L/cycle; (b) 250°C, (1) 1.4×10^8 L; (2) 2.3×10^8 L; heating rates: 8.3°C/s; after reaching 500°C → T const.

L, after previous O_2 dosing at 250°C, 1.3 mbar, 6×10^{10} L, and short evacuation; $T_m \simeq 545$ K (β_1), $T_m = 590$ K (β_2); intensity $\beta_1/\beta_2 = 1.1$ (*7*); and (b) Ag(110) $T_a = 217$°C, $T_m \simeq 570$ and 610 K, intensity $\beta_1 < \beta_2$. With increasing chlorine coverage both peaks shift to lower temperatures and merge to a single broad peak at about 580 K (*2, 3*). The difference in the activation energy for desorption of β_1 and β_2 is 15 and 12 kJ/mol in Experiments a and b, respectively.

In an earlier study (*12*) we found: Ag foil, $T_a = 227$°C, heating rate 4.2 K/s, unresolved single peak, $T_m = 620, 610, 600, 590, 580$ K at Θ O(a) = 0.12, 0.15, 0.20, 0.29, 0.34. The T_m shift corresponds to second-order O(a) desorption and to an increased contribution of the lower temperature β peak to the merged peak at higher coverage. It is interesting to note that oxygen as a self-promoter and chlorine show similar effects.

Oxygen dosing at room temperature and above 200°C leads to peak shifts to higher and lower temperatures, respectively. At $T_a = 150$°C (Fig. 1a) obviously both effects compensate.

Refering to Fig. 1b, it is seen that at sufficiently high temperatures of adsorption and large doses, in addition to the β peak a γ peak ($T_m \cong 800$ K) is shown. This peak is assigned to dissolved lattice oxygen O^{2-}(d) (*7*) ($E^*_{des} > 200$ kJ/mol, isotope exchange (*11*), diffusion kinetics). With increasing doses the intensity ratio γ/β increases.

For an experiment at $T_a = 350$°C, $p_{O_2} = 0.2$ mbar (not shown) a plot of γ-peak intensity versus the square root of the dosing time resulted in a straight line, indicating that diffusion processes are involved. From the total amount O_2 desorbed in consecutive TPD runs after 36 h dosing, a thickness of eight atomic layers has been estimated on the basis of composition of Ag_2O for the surface oxide.

2. *Reactivity of Oxygen Species*

On the basis of TPD findings, catalytic experiments were carried out in such a way that the reactivity of the different oxygen species could be tested. After standard O_2 treatment (see below), suitable choice of the evacuation temperature served to single out the desired species. The results are summarized in Table 1. In experiment 1, β and γ oxygen are present and possibly at small concentrations of α_2, formed on admission of the educt mixture. Relatively high selectivity is observed. In the presence of β and γ oxygen (Experiment 2), pure ethene as educt leads to CO_2 and some EO. The latter is due to reaction with β oxygen formed by the standard treatment. This experiment indicates that α_2 oxygen is not required for selective oxidation. In Experiment 3, only γ oxygen is available and on admission of ethene, only CO_2 is produced at $T > 250$°C. Finally, starting with an oxygen-free Ag surface (Experiment 4), β oxygen and possibly α_2 can be generated by the O_2/E educt mixture. Although γ subsurface oxygen is negligible, EO is formed in addition to CO_2, although only with low selectivity.

3. *Conditioning of the Ag Catalyst*

In order to obtain reproducible kinetic results and stable activity and selectivity,

TABLE 1

Reactivity of Different Oxygen Species

Educt: p_E = 4.9 mbar + O_2 + Ar, p_{tot} = 26 mbar
TPR: 1°C/min
Species: $\alpha_2 = O_2^{\delta-}$(a), $\beta = O^{\Delta-}$(a), $\gamma = O^{2-}$(d)

No.	Pretreatment	Evacuation (10^{-7} mbar) T (°C)	Oxygen Species	Educt O_2/E	Reaction type	T (°C)	Products
1	Standard O_2	250	(α_2), β, γ	1.1 : 1	Batch	250	CO_2, EO
					TPR	$100 \leqq T < 440$	S_{EO} (250°C) = 0.61
2	Standard O_2	190	β, γ	Only E	TPR	$100 \leqq T < 440$	CO_2, EO
3	Standard O_2	300	γ	Only E	TPR	$100 \leqq T < 440$	CO_2, $T > 250$°C
4	H_2 Reduction, 10 mbar, 500°C, 15 h	250	(α_2), β	1.1 : 1	Batch	250	CO_2, EO, S_{EO} (250°C) ≅ 0.1

the following pretreatment was adopted to adjust the oxidation state of the Ag surface. Initially the Ag foil was annealed at 500°C, then treated with H_2 (10 mbar, 500°C, 15 h) and again annealed under vacuum (10^{-8} mbar). Between successive kinetic experiments the following standard pretreatment was performed. At the end of a run the reactor was evacuated at 250°C and subsequently the catalyst annealed at 500°C, 15 h, 10^{-8} mbar. For the next experiment the Ag surface was loaded with O_2 (10 mbar, 350°C, 4 h), followed by ½-h evacuation at 250°C, 10^{-7} mbar. Then the reaction temperature was adjusted and the educt mixture admitted.

Figure 2 illustrates that after H_2 reduction of the catalyst, several standard pretreatments and reaction cycles are required to reestablish the previous selectivity. This is achieved by the formation of an oxidic surface layer.

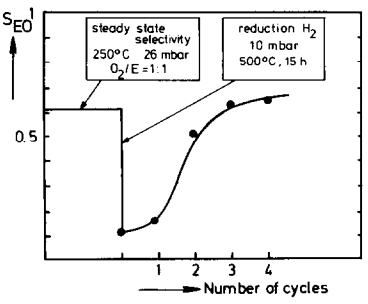

FIG. 2. Conditioning of Ag catalyst surface.

4. Kinetic Measurements

The following series of measurements were carried out: (i) non-steady-state batch experiments, isothermal as well as temperature-programmed reaction (TPR) and (ii) steady-state flow experiments. For the purpose of comparison, the total pressure was the same in all experiments (26 mbar) and one of the educt partial pressures was kept constant, the balance being made up by Ar.

The conversion of ethene and the fractional selectivity for ethene oxide are defined as

$$C_E = \frac{p_E^0 - p_E}{p_E^0} \quad (1)$$

$$S_{EO,E} = \frac{p_{EO}}{p_{EO} + 0.5p_{CO_2}} = \frac{r_{EO}}{r_{EO} + 0.5r_{CO_2}}, \quad (2)$$

where p_E^0 is the initial partial pressure and r_{EO} and $0.5r_{CO_2}$ are the reaction rates for selective and total oxidation.

4.1. Isothermal batch experiments. In Fig. 3 partial pressures are shown as a function of time for O_2-deficient (a) and O_2-ex-

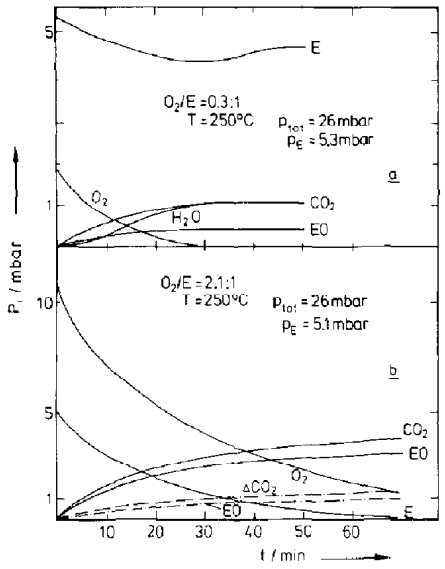

FIG. 3. Isothermal batch experiments. O_2-deficient (a) and O_2-excess (b) educt mixtures. Broken lines: added CO_2, 2.3 mbar.

cess (b) educt mixtures. In the former case, when O_2 is completely consumed p_E exhibits a minimum. Selective and total oxidation always starts immediately without an induction period. Remarkably, H_2O could also be quantitatively determined by means of the omegatron mass spectrometer. Although at the beginning the increase of p_{H_2O} is retarded due to adsorption, the stoichiometric partial pressure is reached eventually, within experimental error. The H_2O curves are not shown in further diagrams.

Both the conversion and selectivity increase with increasing O_2/E ratio (Fig. 4). During the course of an experiment S_{EO} remains constant.

4.2. TPR experiments. The temperature dependence of the catalytic reaction has been studied by means of the TPR technique, using an appropriate heating rate of 1°C/min. For an O_2-deficient educt mixture (Fig. 5a) the p_E curve exhibits a minimum, coinciding with a maximum of EO when O_2 is completely consumed. Comparable results were obtained by van Santen and de Groot (*8*). At a larger O_2/E ratio (Fig. 5b) the EO maximum is shifted to a higher temperature e.g., from ≅250 to 330°C.

Conversion and selectivity as a function of temperature are shown in Fig. 6. In order to test whether subsequent oxidation of EO must be taken into account, a TPR oxidation experiment was carried out with EO (not shown). After standard O_2 pretreatment of the catalyst, an O_2/EO = 2 : 1 mixture (p_{tot} = 26 mbar, P_{EO} = 4 mbar, +Ar)

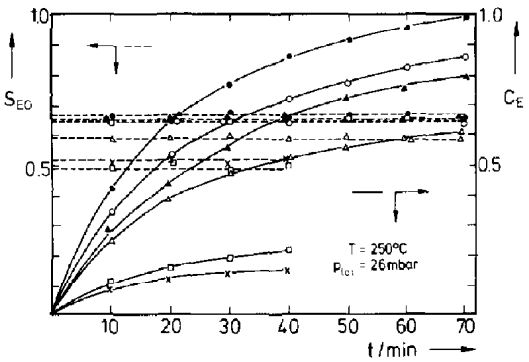

FIG. 4. Conversion and selectivity for isothermal batch experiments. p_{O_2} = 4.4 mbar; O_2/E—▲, 1.8 : 1; △, 1.1 : 1; ×, 0.2 : 1; p_E = 5.3 mbar; O_2/E—●, 3 : 1; ○, 2.1 : 1, □, 0.3 : 1.

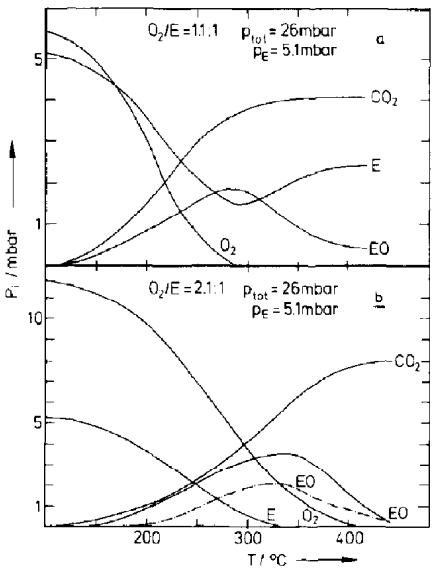

FIG. 5. TPR experiments. O_2-deficient (a) and O_2-excess (b) educt mixtures. Broken line: added CO_2, 2.3 mbar.

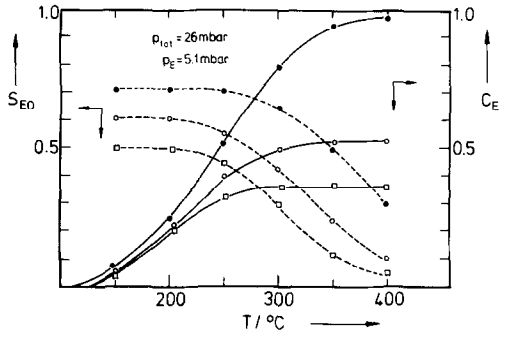

FIG. 6. Conversion and selectivity as a function of temperature. O_2/E—●, 2.9 : 1; ○, 1.1 : 1; □, 0.6 : 1.

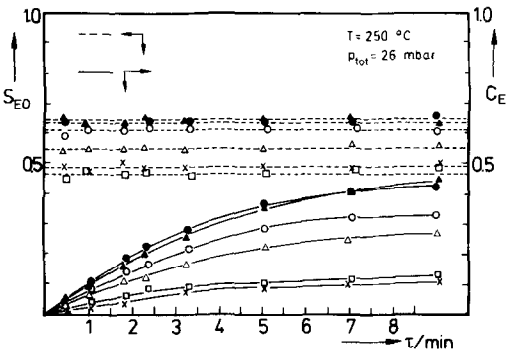

FIG. 8. Conversion and selectivity as a function of contact time. p_{O_2} = 4.5 mbar: O_2/E—▲, 1.8 : 1; △, 1 : 1; ×, 0.3 : 1; p_E = 5.1 mbar: O_2/E—●, 4.1 : 1; ○, 2.3 : 1; □, 0.3 : 1.

was admitted to the reactor at 100°C, followed by TPR at 1°C/min. Subsequent oxidation is negligible at 250°C and occurs to an appreciable extent only above $T \approx 300$°C under the conditions studied here.

4.3. Steady-state flow experiments. In a series of experiments with various educt mixtures the measurements were carried out at increasing contact times $\tau = V_R/\dot{V}$, where V_R is the reactor volume and $\dot{V}$ the volume gas velocity. Subsequent control experiments at smaller τ values confirmed the reproducibility. Steady-state conditions were established within 5–10 min. At small values $\tau < 1.5$ min, i.e., at low conversion $C_E < 0.15$, the partial pressures p_{EO} and p_{CO_2} are a linear function of the contact time, thus enabling the evaluation of reaction rates (Fig. 7).

Conversion and selectivity as a function of contact time are shown in Fig. 8. C_E increases monotonously with τ; however, C_E is smaller even at the longest contact time (9 min) than in the batch experiments at corresponding p_{O_2}/p_E (Fig. 4). On the other hand comparable to those experiments, S_{EO} is independent of the contact time and increases with O_2/E ratio.

4.4. Influence of CO_2. The inhibiting effect, already shown in Figs. 3 and 5, with respect to the degree of conversion as a function of temperature is further demonstrated in Fig. 9. Remarkably, selectivity is not affected under the stated reaction conditions. At 250°C in the range $0 \leqq p_{CO_2}$ (mbar) $\leqq 2.3$, C_E decreases while S_{EO} remains constant.

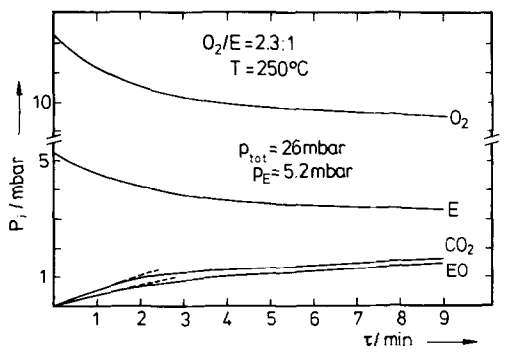

FIG. 7. Steady-state flow experiment.

IV. KINETIC MODELING

The kinetic measurements were evaluated by means of the Horiuti–Temkin formalism (*15*). This procedure is particularly suitable for the treatment of complex catalytic reactions and avoids oversimplifying assumptions. In this way Temkin has studied in detail the silver-catalyzed ethene oxidation (*15*). The kinetic model suggested here differs in some fundamental aspects and is based on the following experimental findings.

(i) IR results (*16*), TRP experiments (*4a, 7*), kinetic studies with different individual oxygen species (*17*, Table 1), and isotope

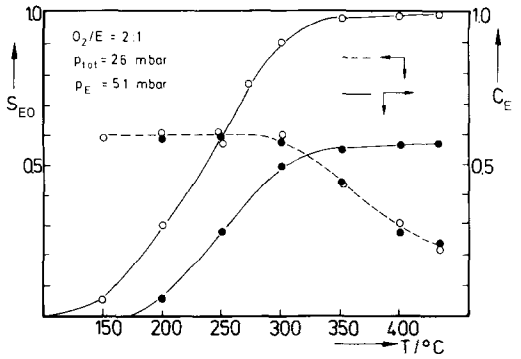

FIG. 9. Inhibiting effect of CO_2. ●, p_{CO_2} = 2.3 mbar; ○, p_{CO_2} = 0.

studies (*8*) are strong evidence that chemisorbed atomic oxygen, $O^{\Delta-}$(a), is operative as the reactive surface species.

(ii) Molecularly chemisorbed oxygen, O_2 (a), is not directly involved in the primary catalytic step (*4, 5, 7, 8*), however, can act as a precursor for the reactive atomic oxygen species.

(iii) Dissolved oxygen, O^{2-}(d), incorporated in the lattice of an oxidic surface layer and acting as a self-promoter is a prerequisite for a stable oxidation state of the catalyst surface and high selectivity (*17, 6, 7, 5,* and Table 1).

(iv) Various findings, e.g., IR (*16*) and isotope (*18*) studies, suggest that both the selective and total oxidation proceed via a common primary surface intermediate. Further evidence is the nearly same apparent activation energy for both reaction routes (*19, 20, 2a, 5*).

(v) Total oxidation can occur along two routes: via isomerization of the primary EO intermediate and via oxidation of chemisorbed E (see, e.g., (*5*)).

(vi) Further oxidation for EO to CO_2 and H_2O becomes noticeable only above ≅ 300°C (see Section III, 4.2).

(vii) The selectivity, S_{EO}, increases with increasing p_{O_2} at constant p_E and decreases with rising p_E at constant p_{O_2} (Figs. 4 and 8).

(viii) With rising temperatures S_{EO} decreases above 250°C depending on p_{O_2}/p_E (Fig. 6).

(ix) In batch experiments, *E* desorbs after complete O_2 consumption (Figs. 3 and 5).

(x) Addition of CO_2 inhibits the reaction, however, does not affect the selectivity under the conditions studied here (Fig. 9).

The overall reaction equations for selective and total oxidation

$$C_2H_4 + \tfrac{1}{2}O_2 = C_2H_4O$$

$$C_2H_4 + 3O_2 = 2CO_2 + 2H_2O$$

are linear combinations of elementary steps, each of which is adjusted by a stoichiometric number in such a way that for various possible reaction routes, the intermediates cancel out. A unique solution of the system of equations can only be obtained if the folowing relation holds

$$P = S + W - I, \qquad (3)$$

where *P*, *S*, *W*, and *I* are the number of routes, elementary steps, balance equations, and surface intermediates, respectively (*15*). In the following model reactive catalytic centers (*) are envisaged as sites of partially charges $Ag_n^{\Delta+}$, embedded in the oxygen-loaded silver surface. The symbols →, ⇌, and ⇋ refer to irreversible, reversible, and equilibrium reactions. Intermediates adsorbed on active centers are designated $*{\cdot}I$; otherwise the symbol of components refers to the gaseous state. The electrical charges are not indicated for simplicity reasons and because these are not reliably known. It should be realized, however, that charge transfer in the adsorption and desorption steps as well as in O_2(a) dissociation is involved.

Kinetic Model

The mechanism comprises 9 intermediates (inclusively the vacant catalytic site), 11 elementary steps, and 1 balance equation of the intermediates. According to Eq. (3) this corresponds to three independent reaction routes as presumed in the kinetic model. In this sense the model is in itself

	Elementary step	Stoichiometric number			Surface process
		$P^{(1)}$	$P^{(2)}$	$P^{(3)}$	
1.	$O_2 + * \rightleftharpoons * \cdot O_2$	$\frac{1}{2}$	$\frac{1}{2}(1-x)$	0	O_2 chemisorption
2.	$* \cdot O_2 + * \rightleftharpoons 2 * \cdot O$	$\frac{1}{2}$	$\frac{1}{2}(1-x)$	0	O_2(a) dissociation
3.	$C_2H_4 + * \cdot O \rightarrow * \cdot O \cdot C_2H_4$	1	$1-x$	0	E chemisorption common interm. $P^{(1)}$
4.	$* \cdot O \cdot C_2H_4 \rightarrow * + C_2H_4O$	1	0	0	EO desorption
5.	$* \cdot O \cdot C_2H_4 \rightarrow * \cdot O \cdot CHCH_3$	0	$1-x$	0	Isomerization
5′.	$* \cdot O \cdot CHCH_3 + \frac{5}{2}O_2 \rightarrow * + 2CO_2 + 2H_2O$	0	$1-x$	0	Total oxidation $P^{(2)}$
6.	$CO_2 + * \cdot O \not\rightleftharpoons * \cdot O \cdot CO_2$	0	0	0	CO_2 inhibition
7.	$H_2O + * \cdot O \not\rightleftharpoons * \cdot O \cdot H_2O$	0	0	0	H_2O inhibition
8.	$C_2H_4 + * \rightleftharpoons * \cdot C_2H_4$	0	0	x	E chemisorption
9.	$* \cdot C_2H_4 + O_2 \rightarrow * \cdot C_2H_4 \cdot O_2$	0	0	x	Total oxidation $P^{(3)}$
9′.	$* \cdot C_2H_4 \cdot O_2 + 2O_2 \rightarrow * + 2CO_2 + 2H_2O$	0	0	x	Total oxidation $P^{(3)}$

consistent. As generally accepted the consecutive steps (5′) and (9′) are assumed to be very fast. The oxygen for reactions (5′), (9), and (9′) is considered to be supplied from the gas phase although adsorbed oxygen may be involved. The notation of the intermediate $* \cdot C_2H_4 \cdot O_2$ is simply formal and should not suggest a peroxy compound. Adsorption equilibrium for CO_2 and H_2O at a reaction temperature of 250°C accounts for the inhibiting effects of these reaction products. Readsorption of EO is not included since it would merely lead to a longer residence time of the $* \cdot O \cdot C_2H_4$ intermediate and to further oxidation according to steps (5) and (5′). As mentioned EO oxidation has not been found under the given conditions.

V. EVALUATION OF KINETIC PARAMETERS

The areal reaction rate is defined as

$$r = \frac{1}{\nu_i} \cdot \frac{1}{A} \frac{V_R}{RT} \cdot \frac{dp_i}{dt} \qquad \frac{\text{mol}}{\text{cm}^2\,\text{s}}, \tag{4}$$

here ν_i is the stoichiometric coefficient of component i, the surface area, here the geometric surface, $A = 200$ cm^2, and the reactor volume $V_R = 30$ cm^3. Alternatively the reaction rates can be expressed in terms of a turnover frequency (number) (TON), i.e., the number of reacted molecules per site and unit time:

$$\text{TON} = r \cdot \frac{N_A}{L} \qquad \text{molecules/site} \cdot \text{s}^{-1} \tag{5}$$

where N_A is the Avogadro number and L the number of reactive sites/cm^2, $L = 1.3 \times 10^{15}$ Ag atoms/cm^2.

A typical plot of TON vs the educt pressures $p^0_{O_2}$ at p^0_E = const, and p^0_E at $p^0_{O_2}$ = const is shown in Fig. 10 for flow experiments at low conversions ($C_E < 0.15$). It has been shown (*9*) that the results of flow experiments agree with those of batch experiments if in the latter case the initial reaction rates are used.

1. Steady-State Analysis

The rate r_s of the sth elementary step is given by the relation

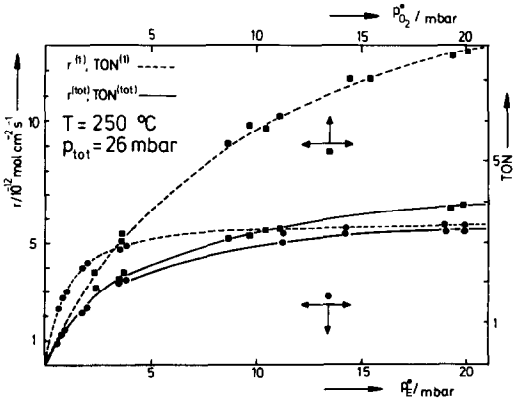

FIG. 10. Rate and TON of selective and total oxidation vs ■ $p^0_{O_2}$ at p^0_E = const = 5.1 mbar and vs ● p^0_E at $p^0_{O_2}$ = const = 4.5 mbar. (TON in 10^{-3} molecules site^{-1} · s^{-1}.)

$$r_S = \sum_{P=1}^{P} \nu_S^{(P)} \cdot r^{(P)} \tag{6}$$

where $r^{(P)}$ is the rate along a reaction route P and $\nu_S^{(P)}$ is the stoichiometric number of the relevant step (*15*).

The application of Eq. (6) to the model leads to the following relations, where k_s, K_s, and $[X_i]$ denote the relevant rate constants, equilibrium constants, and mole fractions of intermediates, respectively. $[X_i] = N_i/L$, where N_i = molecules of intermediate and L = sites both per unit area.

$$\sum_{i=1}^{i} [X_i] = 1. \tag{7}$$

In the derivation (see Appendix) two approximations are made:

(i) For the fast and irreversible steps (5′, 9′) the mole fractions of the intermediates are neglected in the balance equation (7).

(ii) The rate of desorption in step (1) is considered as small in comparison to the rate of formation of the primary intermediate in step (3):

$$r_{-1} = k_{-1}[* \cdot O_2] \ll r_3 = k_3 p_E[* \cdot O].$$

This assumption appears to be justified since the surface concentration of the chemisorbed molecular oxygen is known to be small (*24*) and the reactivity of the crucial atomic oxygen species can be expected to be relatively large.

Thus one obtains the following for the reaction rates for selective and total oxidation as well as for ethene oxide selectivity:

$$r_{epox} = \frac{V_R}{ART}\frac{dp_{EO}}{dt} = r^{(1)} = \frac{k_3 k_4}{k_4 + k_5} p_E \left(1 - \frac{k_1}{k_2} p_{O_2}\right) \cdot \frac{1}{F} \tag{8}$$

$$r_{tot} = \frac{V_R}{ART}\frac{1}{2}\frac{dp_{CO_2}}{dt} = (1 - x)r^{(2)} + xr^{(3)} \tag{9}$$

$$= \frac{1}{F}\left(1 - \frac{k_1}{k_2} p_{O_2}\right)\left[\frac{k_3 k_5}{k_4 + k_5} p_E + \frac{k_3 k_8 k_9}{2k_1(k_9 p_{O_2} + k_{-8})} p_E^2\right] \tag{10}$$

$$F = k_3 p_E \left(\frac{1}{2k_1 p_{O_2}} + \frac{k_8}{2k_1(k_9 p_{O_2} + k_{-8})}\frac{p_E}{p_{O_2}} + \frac{1}{k_4 + k_5}\right) + \frac{2k_1 k_{-2}}{k_2 k_3}\frac{p_{O_2}}{p_E} + 1 + K_6 p_{CO_2} + K_7 p_{H_2O} \tag{11}$$

$$\frac{1}{S_{EO}} = \left(1 + \frac{k_5}{k_4}\right)\left[1 + \frac{k_8}{2k_1}\frac{p_E}{p_{O_2}}\frac{\frac{k_9}{k_{-8}} p_{O_2}}{1 + \frac{k_9}{k_{-8}} p_{O_2}}\right]. \tag{12}$$

2. *Non-Steady-State Analysis*

For the evaluation of batch experiments the differential equations for all educts, products, and intermediates are formulated, describing the change of partial pressure and mole fractions of intermediates with time. It can be shown that with some plausible assumptions (see Appendix) the system of differential equations lead to the same results for r_{epox}, r_{tot}, and S_{EO} as derived above for steady-state conditions.

3. *Selectivity Behavior*

The change of the reciprocal selectivity (Eq. (12)) as a function of the ratio of the initial partial pressures $p_E^0/p_{O_2}^0$ is shown in Fig. 11. It can be seen that the following relations hold:

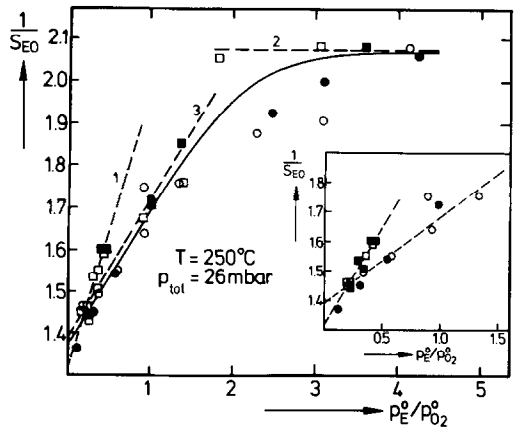

FIG. 11. Reciprocal selectivity vs educt ratio $p^0_E/p^0_{O_2}$ at p^0_E = const = 5.1 mbar: ■, flow experiments; □, batch experiments; and at $p^0_{O_2}$ = const = 4.5 mbar: ●, flow experiments; ○, batch experiments.

(i) For flow and batch experiments with p^0_E = const at sufficiently high p_{O_2}, i.e., $(k_9/k_{-8})p^0_{O_2} \gg 1$ the slope of the straight line is $(1 + k_5/k_4) \cdot k_8/2k_1$ and the intercept:

$$(1 + k_5/k_4). \tag{13}$$

This linear relation of $1/S_{EO}$ holds up to $p^0_E/p^0_{O_2} \approx 0.5$.

(ii) For sufficiently small $p^0_{O_2}$ at p^0_E = const, i.e., $(k_9/k_{-8})p^0_{O_2} \ll 1$, the experimental points approach the constant limiting value of $1/S_{EO}$:

$$\lim_{p_{O_2}\to 0} \frac{1}{S_{EO}} = \left(1 + \frac{k_5}{k_4}\right)\left(1 + \frac{k_8 k_9}{2k_1 k_{-8}} p^0_E\right). \tag{14}$$

(iii) For flow and batch experiments with $p^0_{O_2}$ = const, a linear relation between $1/S_{EO}$ and $p^0_E/p^0_{O_2}$ is to be expected for all ratios of initial educt pressures, with intercept

$$\left(1 + \frac{k_5}{k_4}\right)$$

and slope

$$\left(1 + \frac{k_5}{k_4}\right)\frac{k_8}{2k_1}\frac{(k_9/k_{-8})p^0_{O_2}}{1 + (k_9/k_{-8})p^0_{O_2}}. \tag{15}$$

The deviation from a straight line above $p^0_E/p^0_{O_2} > 1.5$ may be attributed to increasing blockage of reactive sites and/or changing electronic properties by ethene adsorption.

The dependence of the selectivity on the initial educt pressure of $p^0_{O_2}$ at p^0_E = const and p^0_E at $p^0_{O_2}$ = const, is illustrated in Fig. 12 for batch and flow experiments. While the p_{O_2} dependence is correctly described by the kinetic model according to Eq. (12), this is true for the p^0_E dependence only up to about 6 mbar. At higher p^0_E pressures and const $p^0_{O_2}$ = 4.5 mbar the selectivity remains practically constant.

4. *Determination of Rate Constants*

From the relations (13) to (15) the following ratios of rate constants were obtained for a reaction temperature of 250°C:

$$\frac{k_9}{k_{-8}} = 0.31 \pm 0.15 \text{ mbar}^{-1};$$

$$\frac{k_5}{k_4} = 0.33 \pm 0.03;$$

$$\frac{k_8}{2k_1} = 0.50 \pm 0.02.$$

Using these ratios and the relevant initial educt pressures all rate constants can be

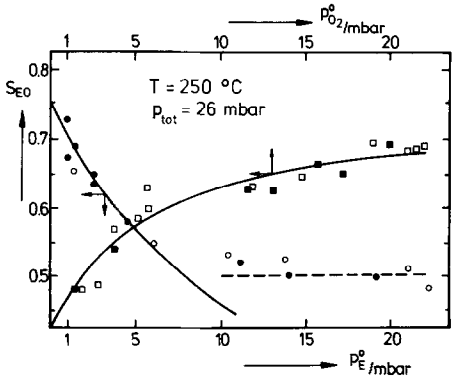

FIG. 12. Dependence of selectivity on educt partial pressures at p^0_E = const = 5.1 mbar: ■, flow experiments; □, batch experiments, and at $p^0_{O_2}$ = const = 4.6 mbar: ●, flow experiments; ○, batch experiments. ——, calculated according Eq. (15) – – –, observed constant S_{EO} for $p^0_E > 10$ mbar.

evaluated by means of the matrix method and the criterion of least squares of errors. It should be pointed out that this treatment of the experimental data is based on the underlying kinetic model and is not a matter of fitting results by means of a sufficient number of constants without physical meaning.

$k_1 = 0.19 \pm 0.01$; $k_3 = 0.76 \pm 0.07$; $k_8 = 0.19 \pm 0.01$;
$k_9 = 0.19 \pm 0.06$; k_1, k_3, k_8, k_9 [10^{-11} mol cm^{-2} s^{-1} mbar^{-1}];
$k_2 = 7.79 \pm 1.20$; $k_{-2} = 2.81 \pm 0.48$; $k_4 = 3.95 \pm 0.28$;
$k_5 = 1.32 \pm 0.07$; $k_{-8} = 0.63 \pm 0.12$; k_2, k_{-2}, k_4, k_5, k_{-8} [10^{-11} mol cm^{-2} s^{-1}]

Only the sum of the adsorption equilibrium constants K_6 and K_7 could be evaluated: $K = K_6 + K_7 = 4.0 \pm 1.0$ mbar^{-1}.

5. Activation Energy

Since the kinetic measurements were mainly concerned with isothermal studies at a reaction temperature of 250°C, it was attempted to obtain information on the activation energies from the TPR experiments. Introduction of the heating rate $\beta = dT/dt$ into Eq. (4) leads to

$$r = \frac{1}{\nu_i}\frac{1}{A}\frac{V_R}{RT}\beta\frac{dp_i}{dT} = k'f(p_i) = k_0'f(p_i)e^{\frac{-E^*}{RT}}. \quad (16)$$

In this way the reaction rate r can be calculated from the experimental dp_i/dT data: k' denotes the rate constant of the overall selective or total oxidation reaction and $f(p_i)$ the partial pressure term expressed, e.g., as a power rate law or Hougen–Watson type of equation; E^* = apparent activation energy, and k_0' = preexponential factor.

On the assumption that the partial pressure term can be considered as approximately constant in the range of relatively low temperatures, i.e., low conversion, a linear relation between ln r and $1/T$ can be expected. In fact for TPR experiments in the temperature range 150–230°C straight lines were obtained in the Arrhenius plot. The intercepts are somewhat different, according to the $f(p_i)$ term which is given by the initial educt partial pressures. The slopes of the corresponding straight lines are, however, not affected. For epoxidation and total oxidation the same activation energy of about 35 kJ/mol was obtained.

VI. DISCUSSION

Recent studies (*4, 5, 7, 8*) are in agreement with the earlier IR findings (*16*) that adsorbed atomic oxygen is essentially the reactive species and have shown that subsurface oxygen is required for high selectivity. Dissolved oxygen acts as a self-promoter, similar to the effect of chlorine (*5*). Campbell's reinterpretation of his data also approaches this concept as far as O(a) is concerned (*1c*). In principle, it cannot be excluded that O(a) recombines before reaction to EO; however, van Santen and de Groot (*8*) regard this as unlikely under their experimental conditions. These are similar to those in this paper as far as the p_{O_2} range is concerned. In the absence of any experimental proof for such a reactive O_2(a) species under reaction conditions, the kinetic model has been based on the direct interaction of O(a) with E.

The nature, i.e., the bonding and electrical charge of the reactive O(a) species, is as yet not clear. In this context it is of interest that on polycrystalline Ag (*7*) as well as on Ag(110) (*2, 3*) two adsorption states in the β O(a) TPD range ($\cong$590 K) were identified. In both cases the difference in the activation energy for desorption are about the same $\cong$15 kJ/mol.

Recalling earlier results on the energetics

of oxygen adsorption (*22*), van Santen and de Groot (*8*) suggest the existence of two adsorption states of which monocoordinated O(a) would lead to EO and multicoordinated O(a) to total combustion. Alternatively, it can be envisaged that the less strongly adsorbed of the two exchangeable O(a) species is essentially the reactive species both for selective and total oxidation via a common primary intermediate. The kinetic model suggested here is based on this concept (see Section IV) and the so derived kinetic data agree with the experimental findings.

The important role played by subsurface oxygen has been pointed out by various authors (*17, 21, 7, 8, 5*). Our earlier (*7*) and present results clearly show a TPD peak (γ) at $\cong$800 K after oxygen pretreatment at sufficient high temperature and dosis (see Section III, 1). This species can be assigned to dissolved lattice oxygen, O^{2-}(d), incorporated in an oxidic surface layer. We have suggested (*6, 7*) that Ag_2O, the most stable Ag oxide, exhibiting widely variable stoichiometry acts as a frame work lattice for oxygen uptake and transfer. It may be recalled that Ag_2O surface layers have been repeatedly discussed in connection with the catalytic ethene oxidation (e.g., *15, 16, 23, 26, 3, 1b*).

A γ peak has hitherto not been reported by other authors, except for a recent discussion remark (*5*). The detectability of the dissolved oxygen species may depend on various factors: not high enough TPD temperature, sorption temperature, or dose as well as the use of single crystals instead of polycrystalline Ag. In the latter case accelerated grain boundary diffusion will be involved both in the sorption and TPD process. The composition and thickness of the oxidic surface layer are still questions of vital interest. In addition to promoters these factors are important to the electronic properties of the catalyst. They will control the influence of the underlying silver metal and the electron transfer in the surface processes (*6, 7*).

For the O_2/Ag system 1 to 5 Ag_2O overlayers have been reported on Ag(111) (*1b*) and 8 layers were estimated here under the given conditions (Section III, 1). On the other hand a thickness of only 2 oxide layers was determined by CO titration in ethene oxidation with a Ag/Al_2O_3 catalyst (*25*). The experimental methods may, however, be limited to a certain depth of the surface layer because transport processes are involved. What really matters is the stoichiometry and thickness of the oxidic surface layer of a working catalyst under the conditions of a redox system at the reaction temperature and excess oxygen.

The kinetics of the catalytic ethene oxidation has been repeatedly reviewed (*21, 26*). The experimental data were in some cases fitted to a power rate law, although interpretation of the resulting reaction orders may be difficult or impossible. Frequently a rate equation was derived on the basis of a rate-determining step, e.g., a surface reaction between adsorbed ethene and adsorbed oxygen, and the assumption of Langmuir adsorption isotherms. In order to avoid oversimplifications the present kinetic measurements were evaluated by means of the Horiuti–Temkin formalism (*15*) which the latter author has particularly applied to the catalytic ethene oxidation. The underlying concept used here is, however, significantly different (Section IV).

The selectivity behavior which is, of course, most relevant from the mechanistic as well as practical point of view, will be discussed first. S_{EO} remains constant during the course of batch experiments and is independent of the contact time in flow experiments (Figs. 4 and 8). This indicates a stable oxidation state of the Ag surface and the absence of subsequent EO oxidation. The TPR experiments (Fig. 6) show a decrease of S_{EO} above 250°C and at somewhat lower temperatures with decreasing O_2/E educt ratio. A decrease of the selectivity at higher temperatures has been generally found, depending specifically on the type of

catalyst, its pretreatments, and the reaction conditions.

From the expressions derived for the reaction rates of epoxidation (Eq. (8)) and total oxidation (Eq. (9)), the EO selectivity can be calculated (Eq. (12)). It can be seen from Fig. 12 that the increase of S_{EO} with rising educt $p^0_{O_2}$ is correctly described by the model calculations over the whole range $p^0_{O_2}$ (mbar) $\leqq 20$. With increasing p_E the influence of reaction route (3) becomes noticeable. As a function of p^0_E the selectivity decreases correspondingly to Eq. (12) up to about 6 mbar, i.e., in the range of educt ratios $0.75 \leqq p^0_{O_2}/p^0_E \leqq 4.5$. At higher p^0_E the calculated values would be too small compared with the experimental, virtually constant selectivity. This may be attributed to saturation of the catalyst surface with adsorbed ethene. At sufficiently high p_E the rates of both selective and total oxidation become practically constant (Fig. 10). This has also been found, e.g., in Ref. (*27*).

Considering that no other promoters (Cl, Cs) were used, the observed selectivities up to slightly above 70% are remarkably high. Obviously this is due to the oxygen preconditioning of the catalyst surface whereby dissolved oxygen acts as a self-promoter. From the plot in Fig. 11 according to Eq. (13) an intercept of 1.3 is obtained which represents a maximum EO selectivity of 75% under the given conditions. This limiting value depends only on the ratio k_4/k_5, (Eq. (13)), i.e., the rate constants for desorption of EO and the isomerization of the adsorbed primary oxygen–ethene surface intermediate. It is noteworthy that the model calculations lead to a limiting selectivity on the basis of adsorbed atomic oxygen as the reactive species, forming a common primary intermediate with ethene. As often quoted in the literature a limiting selectivity of 86% results for a mechanism based on a coupling between partial and total oxidation via molecular and atomic oxygen species, respectively (*21a*). Recently, however, distinctly higher selectivities have been reported (>90%) (*28*). According to the mechanism suggested here this can be interpreted as a result of acceleration of reaction step (4), e.g., by modification of the electronic properties of the catalyst surface (chlorine addition, O(d)) resulting in faster electron transfer and by suppression of reaction step (5), e.g., by alkali addition (*5*).

The rate constants (Section V, 4) agree with literature data as far as the order of magnitude is concerned (e.g., *26, 29*). For a detailed discussion it would be necessary to compare corresponding elementary steps. Due to the different reaction schemes this is, however, not feasible. From the present studies k_1 and k_3 turn out to be the smallest rate constants (Section V, 4), leaving aside k_8 for reaction conditions with high excess oxygen when the additional reaction route for total oxidation may be neglected. Thus, it can be concluded that essentially the oxygen adsorption and the formation of the primary common surface intermediate ($* \cdot O \cdot C_2H_4$) can be considered as rate determining for the catalytic oxidation reaction. It should be recalled that the ratio k_4/k_5 is the determining factor for the EO selectivity.

The rate constant k_2 (Section V. 4) refers to the dissociation of adsorbed molecular oxygen under reaction conditions. A direct comparison with the dissociation constants k_{diss} (s^{-1}) for Ag(110) and Ag(111) estimated by Campbell (*1b*) is, however, not possible since (i) the O_2/Ag system is considered in the absence of ethene and (ii) oxygen dissociation in the adsorbed state is treated as a first-order process, whereas in the present suggested model an adjacent vacant surface site is required for reaction step (2).

With reference to Fig. 10 the turnover numbers may be inspected. For instance at 250°C and $p^0_E = 5.1$ mbar, $p^0_{O_2}/p^0_E = 4:1$: TON(EO) $= 8 \times 10^{-3}$ molecules $\cdot$ site^{-1} $\cdot$ s^{-1}, based on the geometric area of the polycrystalline Ag foil. In comparison the following results have been reported for clean Ag(111) surfaces at similar temperatures and total pressures, e.g., $p^0_{O_2}/p^0_E = 4:1$, TON(EO) $= 3 \times 10^{-1}$ (*1a*); $1:1$, $4 \times$

10^{-2} molecules · site^{-1} · s^{-1} (*4d*). These are distinctly larger than the values found here as well as those for high-surface-area supported catalysts (see *1a*). Various factors may be important: ensemble effects on single crystal faces, structure sensitivity of the reaction, and the difficulty in assessing the actual Ag surface area (*1a*).

From the TPR experiments (Section V, 5) an overall apparent activation energy of about 35 kJ/mol was estimated for both epoxidation and total oxidation in the temperature range $150 \leqq T$ (°C) $\leqq 230$. It may be recalled that in this range also the selectivity is constant (Fig. 6). These findings may be interpreted as an indication for a common primary intermediate for both reaction routes, one of the presumptions on which the suggested mechanism is based. Nearly equal activation energies have also been observed by other authors (e.g., *2a, 4b, 5, 19, 20*). Imre (*30*), also using an unpromoted Ag metal foil as catalyst, found $E^*(\mathrm{EO}) = 30.5$ and $E^*(\mathrm{CO_2}) = 37.5$ kJ/mol. On the other hand for high-surface-area supported Ag catalysts widely differing activation energies have been reported, e.g., 30.7 and 36.2 (*31*), close to (*30*), and this work; 77 and 63 (*26*); 61 and 92 (*29*) kJ/mol, respectively. Thus further accurate measurements with well-defined catalysts (texture, promoters, and pretreatment) and under comparable reaction conditions are highly desirable for a more detailed kinetic analysis with respect to the rates and activation energies of the different elementary steps of the catalytic reaction.

Regarding the influence of the reaction products, in particular CO_2, the following results were obtained. The selectivity is not affected by CO_2 as indicated by batch experiments with an oxygen-preconditioned Ag foil at 250°C and as well as TPR experiments up to 440°C (section III, 4.4 and Fig. 9). This is in line with the suggested kinetic model which requires that S_{EO} for an unpromoted Ag catalyst and isothermal conditions is only a function of p_E and p_{O_2} but independent of p_{CO_2} (Eq. (12)). Furthermore, it would imply that partial and total oxidation is inhibited to the same extent by CO_2. This may be another indication for a common primary intermediate. On the other hand the degree of conversion, C_E, decreases with increasing p_{CO_2} (Fig. 9), corresponding to the fact that p_{CO_2} as well as p_{H_2O} appear in the denominator of Eqs. (8) and (9). Interestingly, an increase of EO selectivity by CO_2 has been observed with promoted catalysts (*28, 31*). Also recent studies with Ag single crystals have shown that Cs causes a distinct increase of the otherwise relatively weak CO_2 effect on selectivity (*5*).

VII. CONCLUSION

The kinetic model is based on the following concept: Chemisorbed molecular oxygen is involved as a precursor for the reactive adsorbed atomic oxygen existing in two differently bonded surface species. The less strongly adsorbed O(a) forms a common intermediate with ethene for both selective and total oxidation. An oxidic surface layer, presumably nonstoichiometric Ag_2O, can dissolve oxygen, O(d), which acts as a self-promoter and is a prerequisite for a stable and high EO selectivity. The composition and thickness of the surface oxide on top of the Ag metal determines besides added promoters the electronic properties of the catalyst and thus the rates of electron transfer with the adsorbed species, e.g., for EO desorption. Total oxidation can occur via isomerization of the primary intermediate and in addition via oxidation of primarily adsorbed ethene.

The kinetic results are consistent with this model and indicate that oxygen adsorption and formation of the primary intermediate are the rate-determining steps at sufficiently high educt p_{O_2}/p_E ratios. Under these circumstances the selectivity depends only on the ratio of the rates of EO desorption and isomerization of the intermediate. The kinetic model leads to a maximum selectivity which is determined by this ratio.

APPENDIX

In the steady-state analysis application of

Eq. (6) leads to the following relations for the elementary steps. For the equilibrium steps (6) and (7) $r_s = 0$ in Eq. (6), thus leaving the number of equations and unknowns unchanged. The fast and irreversible steps (5′) and (9′) do not contribute to Eq. (6).

$$\begin{aligned} r_1 &= \tfrac{1}{2}r^{(1)} + \tfrac{1}{2}(1-x)r^{(2)} \\ &= k_1 p_{O_2}[*] - k_{-1}[* \cdot O_2] \\ r_2 &= \tfrac{1}{2}r^{(1)} + \tfrac{1}{2}(1-x)r^{(2)} \\ &= k_2[* \cdot O_2][*] - k_{-2}[* \cdot O]^2 \\ r_3 &= r^{(1)} + (1-x)r^{(2)} = k_3 p_E[* \cdot O] \\ r_4 &= r^{(1)} = k_4[* \cdot O \cdot C_2H_4] \\ r_5 &= (1-x)r^{(2)} = k_5[* \cdot O \cdot C_2H_4] \\ r_8 &= xr^{(3)} = k_8 p_E[*] - k_{-8}[* \cdot C_2H_4] \\ r_9 &= xr^{(3)} = k_9 p_{O_2}[* \cdot C_2H_4]. \end{aligned} \tag{17}$$

From Eq. (17) follows

$$r_4 + r_5 = r_3; \quad 2r_1 = r_3; \quad 2r_2 = r_3; \quad r_8 = r_9. \tag{18}$$

Thus after some rearrangements the mole fractions of the intermediates (Eq. (19)), the reaction rates for selective and total oxidation, as well as the EO selectivity (Eqs. (8) to (12), see Section V), are obtained:

$$[* \cdot O \cdot C_2H_4] = \frac{k_3}{k_4 + k_5} p_E[* \cdot O] \tag{19a}$$

$$[* \cdot C_2H_4] = \frac{k_3 k_8}{2k_1} \frac{p_E^2[* \cdot O]}{p_{O_2}(k_9 p_{O_2} + k_{-8})} \tag{19b}$$

$$[*] = \frac{k_3}{2k_1} \frac{p_E[* \cdot O]}{p_{O_2}} \tag{19c}$$

$$[* \cdot O_2] = \frac{k_1}{k_2} p_{O_2} + \frac{2k_1 k_{-2}}{k_2 k_3} \frac{p_{O_2}[* \cdot O]}{p_E} \tag{19d}$$

$$[* \cdot O] = \frac{1}{F}\left(1 - \frac{k_1}{k_2} p_{O_2}\right), \tag{19e}$$

where F is defined by Eq. (11).

With reference to the supply of reactive adsorbed atomic oxygen (steps 1 and 2), various models involving all possible combinations of irreversible, reversible, and equilibrium steps were systematically treated. Among these variations the model described in Section IV is the most general case.

If for the evaluation of kinetic parameters (see section V, 1) only the approximation (i) is used, the solutions for the reaction rates and selectivity are more complex: In this case data evaluation might only be achieved by numerical fitting methods. Nevertheless, the solution derived for S_{EO} is given:

$$S_{EO} = \frac{1 + \dfrac{k_1 p_{O_2}}{k_{-1}} + \dfrac{k_8 p_E}{k_{-8} + k_9 p_{O_2}}}{\left(1 + \dfrac{k_5}{k_4}\right)\left[1 + \dfrac{k_1 p_{O_2}}{k_{-1}} + \dfrac{k_8 p_E}{k_{-8} + k_9 p_{O_2}}\left[1 + k_9\left(\dfrac{1}{k_{-1}} + \dfrac{1}{k_4 + k_5}\right) + \dfrac{k_9}{k_3 p_E}\left(\dfrac{1}{C} - K_6 p_{CO_2} - K_7 p_{H_2O} - 1\right)\right]\right]}$$

$$C = \frac{1}{2\left[A^2\left(\dfrac{k_1 k_{-2}}{k_{-1} k_2} p_{O_2} + \dfrac{k_3^2 p_E^2}{16 k_{-1}^2}\right) - B^2\right]}\left[\left(\left(A^2 \frac{k_1 k_3}{2k_{-1} k_2} p_E p_{O_2} + 2B\right)^2 + 4\right)^{1/2} - \left(A^2 \frac{k_1 k_3}{2k_{-1} k_2} p_E p_{O_2} + 2B\right)\right]$$

$$A = 1 + \frac{k_{-1}}{k_1 p_{O_2}}\left(1 + \frac{k_8 p_E}{k_{-8} + k_9 p_{O_2}}\right)$$

$$B = 1 + k_3 p_E\left(\frac{1}{k_4 + k_5} - \frac{1}{4k_{-1}} + \frac{3}{4k_1 p_{O_2}}\left(1 + \frac{k_8 p_E}{k_{-8} + k_9 p_{O_2}}\right)\right) + K_6 p_{CO_2} + K_7 p_{H_2O}. \tag{20}$$

Closer inspection of Eq. (20) shows qualitatively the same trend of S_{EO} on variation of p_{O_2} and p_E as Eq. (12). Apart from this, Eq. (20) would allow to account for an increase of S_{EO} with p_{CO_2} and p_{H_2O}.

For the non-steady-state analysis the fol-

lowing assumptions are made in addition to the steady-state treatment:

(i) Bodenstein quasi-steady-state for the intermediates built up in steps (3), (5) and (9). Contrary to the latter two cases, the mole fraction of $* \cdot O \cdot C_2H_4$ must be taken into account in Eq. (7) since step (3) is not followed by a fast reaction.

(ii) Bodenstein quasi-steady-state for the intermediate $* \cdot O$ provided that oxygen supply from the catalyst pretreatment and educt mixture is sufficiently large as is the case under the relevant experimental conditions in this study.

From the carbon and oxygen material balance, two more equations are available, thus enabling a unique solution of the system of equations by means of the method of determinants.

For evaluation of steady-state flow experiments at small conversions it is justified to neglect the terms $K_6P_{CO_2}$ and $K_7P_{H_2O}$ in Eqs. (8) and (9). At higher conversions and in the case of batch experiments the experimental reaction rates are obtained by differentiation of the partial pressure p_i curves vs t best fitted to the analytical function $y = \sum_{n=-2}^{2} a_n x^n$.

ACKNOWLEDGMENTS

Financial support from "Deutsche Forschungsgemeinschaft" an "Fonds der chemischen Industrie" is gratefully acknowledged.

Note added in proof. In a recent paper by S. A. Tan, R. B. Grant, and R. M. Lambert (*J. Catal.* **100,** 383 (1986)), a TPD peak (850 K) assigned to dissolved oxygen has been reported for Ag(111) at high levels of lattice oxygen. Also, drastic effects of increased ethene coverage on the selectivity have been observed and discussed.

REFERENCES

1. Campbell, C. T., (a) *J. Catal.* **94,** 436 (1985); (b) *Surf. Sci.* **157,** 43 (1985); (c) *Surf. Sci. Lett.* **173,** 641 (1986).
2. Campbell, C. T., and Paffett, M. T., (a) *Surf. Sci.* **139,** 396 (1984); (b) *Surf. Sci.* **143,** 517 (1984).
3. Campbell, C. T., and Koel, E. B., *J. Catal.* **92,** 272 (1985).
4. Grant, R. B., and Lambert, R. M., (a) *J. Chem. Soc. Chem. Commun.*, p. 662 (1983); (b) *J. Catal.* **92,** 364 (1985); (c) *Surf. Sci.* **146,** 256 (1984); (d) *Langmuir* **1,** 29 (1985).
5. Grant, R. B., Harbach, C. A. J., Lambert, R. M., and Aun Tan, S., *Faraday Symp. Chem. Soc.* **21,** paper 8 (1986).
6. Haul, R., Hoge, D., Neubauer, G., and Zeeck, U., *Surf. Sci. Lett.* **122,** 22 (1982).
7. Haul, R., Neubauer, G., Fischer, D., Hoge, D., and Zeeck, U., *in* "Proceedings, 8th International Congress on Catalysis, Berlin, 1984," Vol. **3,** p. 265.
8. Van Santen, R. A., and de Groot, C. P. M., *J. Catal.* **98,** 530 (1986), and references therein.
9. Neubauer, G., Dissert. Univ. Hannover (1985).
10. Gentsch, H., *et al., Vak. Techn.* **23,** 230 (1974).
11. Fischer, D., Dissert. Univ. Hannover (1982).
12. Hoge, D., Dipl. thesis, Univ. Hannover (1981).
13. Bowker, M., *Surf. Sci. Lett.* **100,** 472 (1980).
14. Prince, K. C., Paolucci, G., and Bradshaw, A. M., *Surf. Sci.* **175,** 101 (1986).
15. Temkin, M. J., *in* "Advances in Catalysis (D. D. Eley, P. W. Selwood, P. B. Weisz, Eds.), Vol. 28, p. 173. Academic Press, Orlando, FL, 1979.
16. Force, E. L., and Bell, A. T., (a) *J. Catal.* **38,** 440 (1975), (b) *J. Catal.* **40,** 356 (1975), (c) *J. Catal.* **44,** 175 (1976).
17. Backx, C., Moolhuysen, J., Geenen, P., and van Santen, R. A., *J. Catal.* **72,** 364 (1981).
18. Cant, N. W., and Hall, K., *J. Catal.* **52,** 81 (1978).
19. Twigg, G. H., *Proc. Roy. Soc. A* **188,** 92 (1946).
20. Kripylo, P., Mögling, L., Ehrchen, H., Harkanyi, I., Klose, D., and Beck, L., *Chem. Techn.* **31,** 82 (1979).
21. (a) Kilty, P. A., and Sachtler, W. M. H., *Cat. Rev. Sci. Eng.* **10,** 1 (1974); (b) Sachtler, W. M. H., Backx, C., and van Santen, R. A., *Cat. Rev. Sci. Eng.* **23,** 127 (1981), and references therein.
22. Czanderna, A. W., *J. Vac. Sci. Technol.* **14,** 408 (1977).
23. Rovida, G., Pratesi, F., Maglietta, M., and Ferroni, E., *Surf. Sci.* **43,** 230 (1974).
24. Clarkson, R. B., and Cirillo, A. C., *J. Catal.* **33,** 392 (1974).
25. Waugh, K. C., Discussion, remark and reply to (7), Vol. **6,** p. 107 (1984).
26. Dettwiler, H. R., Baiker, A., and Richarz, W., *Helv. Chim. Acta* **62,** 1689 (1979).
27. Guseinov, S. L., Frolkina, I. T., Vasilevich, L. A., Avetisov, A. K., and Gelbshtein, A. I., *Kinet. Katal.* **18,** 1455 (1977).
28. Bryce-Smith, D., Blues, E. T., and de Martinez, B. G., *Chem. Ind. (London)*, p. 717 (1983).
29. Stoukides, M., and Vayenas, C. G., *J. Catal.* **70,** 137 (1981).
30. Imre, L., *Ber. Bunsenges, Phys. Chem.* **74,** 220 (1970).
31. Wiese, K. D., Prauser, G., and Dialer, K., *Ger. Chem. Eng.* **3,** 360 (1980).